CIB-W18/35-7-7

INTERNATIONAL COUNCIL FOR RESEARCH AND INNOVATION IN BUILDING AND CONSTRUCTION

WORKING COMMISSION W18 - TIMBER STRUCTURES

EFFECT OF DISTANCES, SPACING AND NUMBER OF DOWELS IN A ROW ON THE LOAD CARRYING CAPACITY OF CONNECTIONS WITH DOWELS FAILING BY SPLITTING

M Schmid

H J Blaß

University of Karlsruhe

GERMANY

R P M Frasson

Federal University of Espirito Santo

BRAZIL

MEETING THIRTY-FIVE
KYOTO
JAPAN
SEPTEMBER 2002

Effect of Distances, Spacing and Number of Dowels in a Row on the Load Carrying Capacity of Connections with Dowels Failing by Splitting

M. Schmid, H.J. Blaß
University of Karlsruhe, Germany
R.P.M. Frasson
Federal University of Espirito Santo, Brazil

1. Introduction

Joints in timber structures often fail in one of the two brittle modes shown in figure 1.

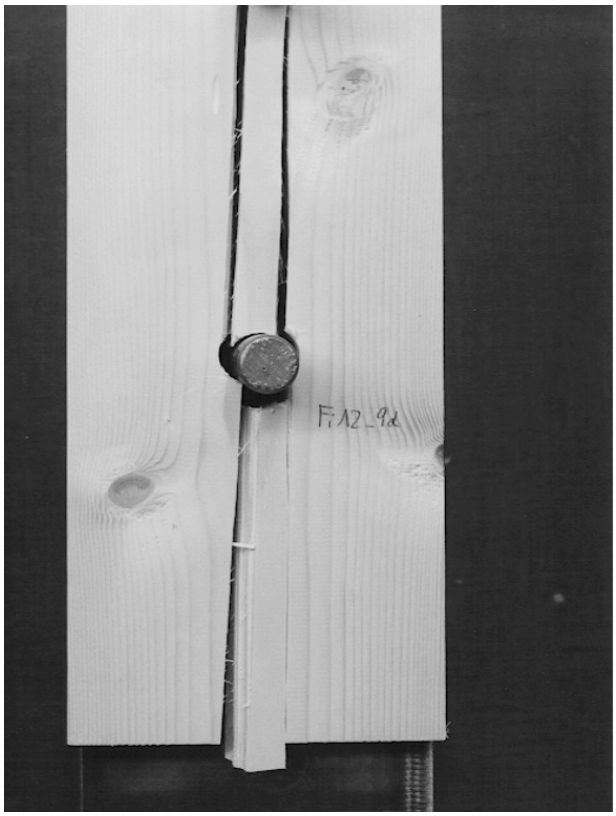

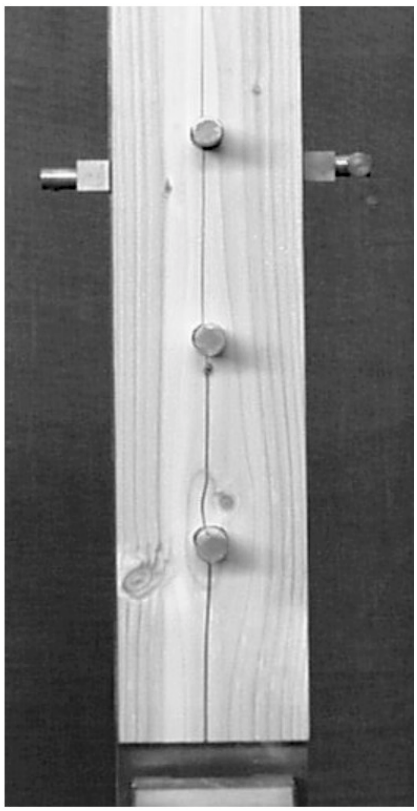

Fig. 1: plug shear failure splitting failure

In order to avoid these brittle failure modes, most timber design codes contain rules based on the experience of craftsmen and results of connection tests in laboratories. These rules mostly consist of prescribed minimum dimensions, such as fastener end and edge distances, fastener spacing, or timber thickness. Regarding these minimum dimensions, no distinction is made between different timber softwood species in many codes. Recent research results e. g. by Jorissen (1998) showed brittle failure modes also in cases where the minimum dimensions were respected. In order to study the influence of the timber species on the splitting tendency, a research project was carried out at Karlsruhe University.

As for economical reasons it is not possible to test all types of fastener using different species and different joint geometry, a mechanical model based on fracture mechanics was developed. In this paper the model for splitting, that was frequently observed in the tests performed both, by Blaß and Schmid (2002) and Masuda (1998), is presented. In terms of fracture mechanics it is a mode I crack extension.

2. Mechanical Model

Stable crack growth in the close neighbourhood of the dowels is often observed (fig. 2), before one of the failure modes shown in figure 1 eventually takes place, leading to an almost complete loss of the joint's strength,.

Fig. 2: crack close to the dowel

The joint area including the stable crack propagation is modelled as a beam on elastic foundation (fig. 3). This model seems to be quite crude, the alternative could be a two- or three-dimensional finite element model. But if the large variation of local timber properties is taken into account, as well as the non-linear stress-strain relation in the area close to the fastener and the orthotropic behaviour, it is reasonable to choose this simple model. Jorissen (1998) first used a similar joint area model. Contrary to the model presented here, Jorissen included no crack extension, he instead compared the tensile stresses perpendicular to the grain at the dowel surface with the tensile strength of the material.

Similar to the approach used by Jorissen (1998) the beam is loaded by a transverse force

$$V = F / 7 \qquad (1)$$

and a moment

$$M = \frac{F/2}{h/2} = \frac{F/2}{a_{4,c}/2} \qquad (2)$$

depending on the embedding behaviour and the dowel load F parallel to the grain.

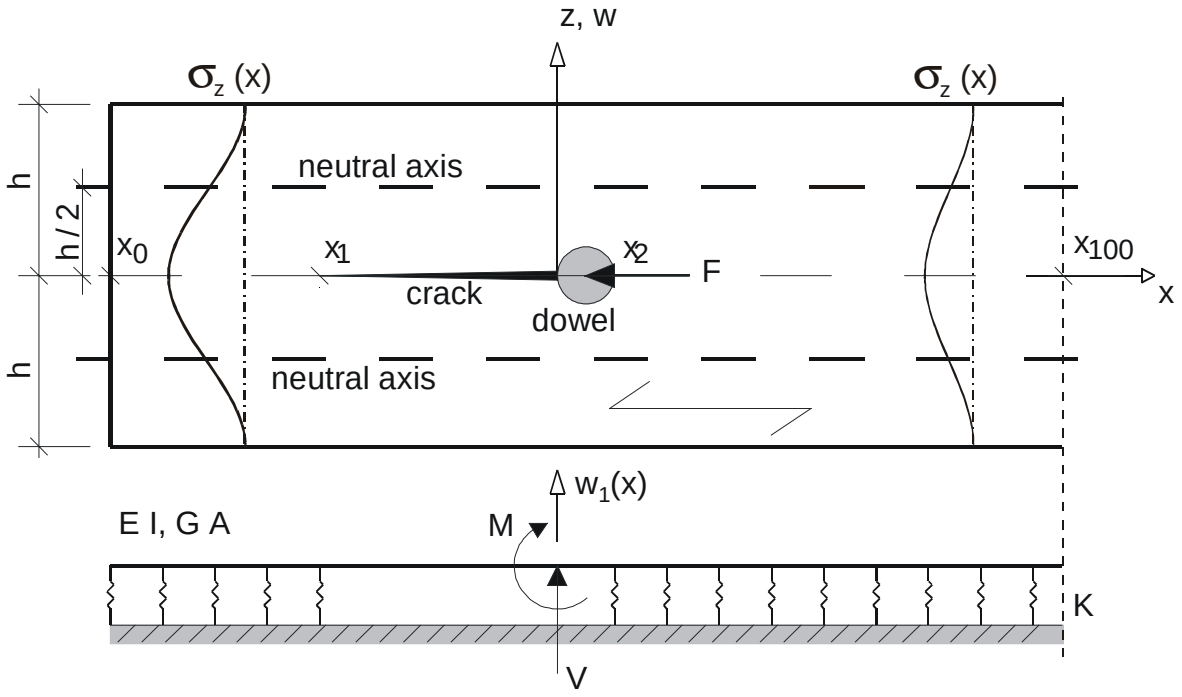

Fig. 3: modelling the cracked joint as a beam on elastic foundation

Assuming a stress distribution perpendicular to the grain $\sigma_z(x,z)$ as shown in figure 3 (Timoshenko and Goodier (1970)), the modulus of foundation K, acting on the neutral axis of the idealised beam, is calculated:

$$\sigma_z(x,z) = \frac{\sigma_z(x,0)}{2} - \left(\frac{3\cdot(-h/2+z)}{2\cdot h} - \frac{2\cdot(-h/2+z)^3}{h^3} \right) \cdot \sigma_z(x,0) \qquad (3),$$

$$w(h/2) = \int_{z=0}^{z=h/2} \varepsilon_{90}(z)\, dz = \int_{z=0}^{z=h/2} \frac{\sigma_z(x,z)}{E_{90}}\, dz = \frac{13\cdot h\cdot \sigma_z(x,0)}{32\cdot E_{90}} \qquad (4)$$

yielding

$$K = \frac{\sigma_z(x,0)\cdot t}{w(h/2)} = \frac{32}{13}\cdot\frac{E_{90}\cdot t}{h} \qquad (5).$$

As the ratio between the depth h of the beam and the length is small, shear deformation is taken into account. Equation (6) follows from equilibrium conditions:

$$\frac{d^4 w_1}{dx^4} - \frac{\kappa\cdot K}{G\cdot A}\cdot\frac{d^2 w_1}{dx^2} + \frac{K\cdot w_1(x)}{E\cdot I} = 0 \qquad (6)$$

A displacement shape function satisfying equation (6) is

$$w_1(x) = e^{\alpha\cdot x}\cdot(C_1\cdot\cos(\beta\cdot x) + C_2\cdot\sin(\beta\cdot x)) + e^{-\alpha\cdot x}\cdot(C_3\cdot\cos(\beta\cdot x) + C_4\cdot\sin(\beta\cdot x)) \qquad (7)$$

with

$$\alpha = \sqrt{\lambda^2 + \frac{\kappa \cdot K}{4 \cdot G \cdot A}}\,,\ \beta = \sqrt{\lambda^2 - \frac{\kappa \cdot K}{4 \cdot G \cdot A}}\,,\ \lambda^4 = \frac{K}{4 \cdot E \cdot I} \qquad (8).$$

Fig. 4 shows the distribution of stresses perpendicular to the grain according to a FE-calculation. The following properties were assumed:

$E_{11} = 420\ N/mm^2$ $E_{22} = 11990\ N/mm^2$ $G_{12} = 743\ N/mm^2$ $\nu_{12} = 0{,}027$

coefficient of friction $\mu = 0{,}339$ $d = 16$ mm $a_{3,t} = 7 \cdot d$ $a_{4,c} = 3 \cdot d$

depth $t = d$

The Poisson coefficient ν_{12} and the coefficient of friction μ are not included in the model according to Figure 3.

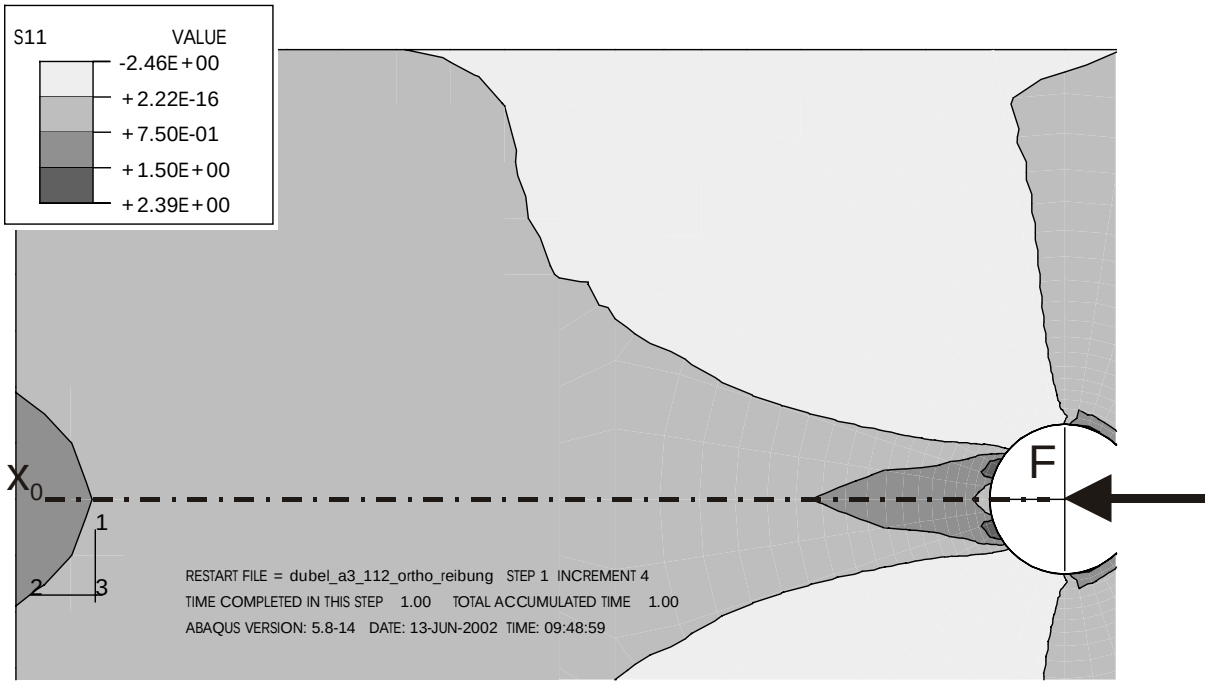

Fig. 4: Stresses perpendicular to the grain according to FE-calculation, coefficient of friction μ = 0,339

Fig. 5 shows the stress distribution perpendicular to the grain along the symmetry axis according to both models. Close to the dowel there is a significant difference between the results. Elsewhere the stresses coincide well. As for the FE-calculation linear-elastic behaviour was assumed, which is not true close to the dowel, and the Poisson coefficient ν_{12} is not very well known either, the precision of the FE-calculation has to be considered with care.

Using the model according to fig. 3 crack propagation Δa is modelled by a prolongation of the non embedded part and an equivalent shortening of the embedded beam parts. Consequently the system becomes weaker resulting in deflections and rotations of the points of actions of M_i and V_i.

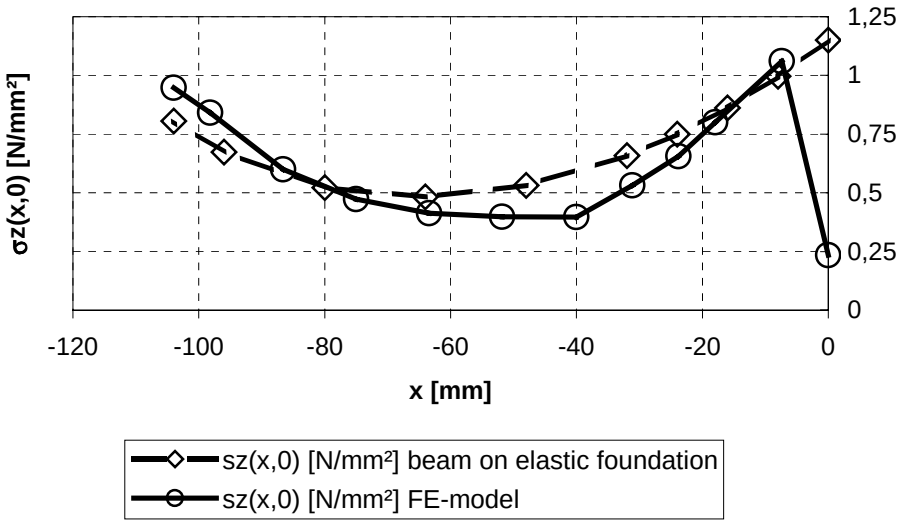

Fig. 5: stresses perpendicular to the grain according to the model and the FE-calculation

The elastic potential is reduced with increasing crack length and the energy release rate is calculated as:

$$G_I = -\frac{\Delta\Pi}{t \cdot \Delta a} = -\frac{\Delta\Pi_V + \Delta\Pi_M}{t \cdot \Delta a} \cdot 2 = \sum_{i=1}^{n} \frac{V_i \cdot \Delta w(x_i)/2 + M_i \cdot \Delta\varphi(x_i)/2}{t \cdot \Delta a} \cdot 2 \qquad (9).$$

The factor 2 in equation (9) results from the symmetry of the joint area, since two beams on elastic foundations form the end of the timber member. For more than one row of fasteners, the model according to figure 3 is only applicable for the outer parts close the member edges, the timber parts between dowel rows are loaded from both sides and basically remain straight. Consequently the energy release rate of mode I for a connection with more than one row is only the half of the value according to equation (9) if crack extension at only one of the outer rows occurs. For this type of joint more often group tear out or shear failure as a mixed mode crack extension (mode I and II) is observed (Quenneville (1998), Mohammad and Quenneville (1999)). A model for calculating the energy release rate G_{II} for this shear failure mode is presented in Blaß and Schmid (2002), but due to a lack of knowledge regarding critical values in mode II and especially for the mixed mode crack extension according to modes I and II a comparison between model and tests remains difficult.

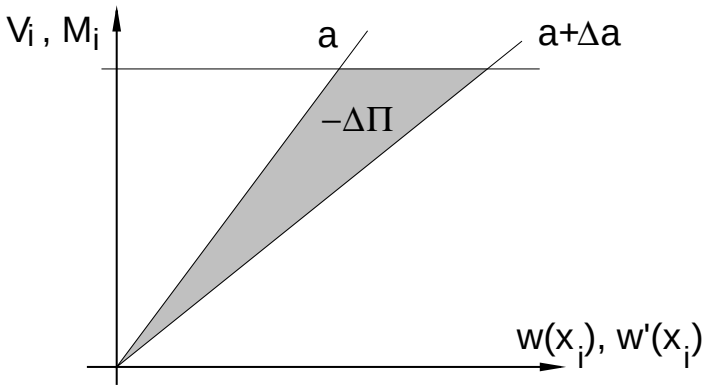

Fig. 6: calculating the energy release rate from the change of the potential ΔΠ

The model shown in figure 3 may easily be extended to a multiple fastener connection. Finally the energy release rate as a criterion for crack propagation can be calculated for different geometry, numbers of fasteners and mechanical properties.

Fig. 7 shows the energy release rates of a model with three dowels and crack extension starting alternatively at the first, the second and the third fastener from the end grain, respectively.

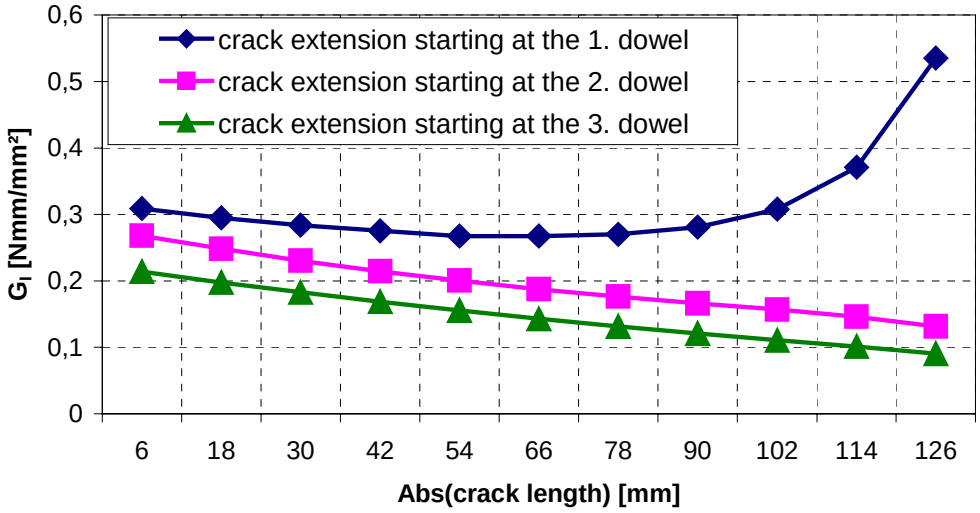

Fig. 7: Energy release rates

Using a critical energy release rate of G_c = 0,214 Nmm/mm² the corresponding load F_c per fastener per shear plane and a crack extension starting from the first fastener depending on the crack length is calculated for a timber thickness of 1 mm (fig. 8).

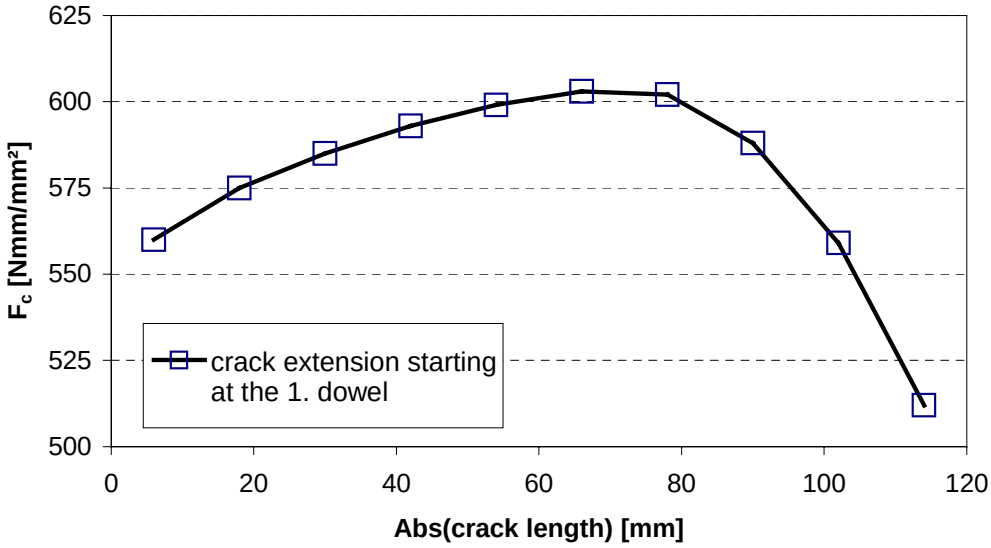

Fig. 8: critical load F_c

The diameter used for the results presented in fig. 7 and 8 was d = 24 mm. Obviously stable crack growth occurs until a crack length of a ≈ 3·d is reached. This was also observed in tests.

3. Results

With models, as e.g. shown for a joint with one fastener in figure 3, calculations of the energy release rate were performed assuming a crack extension starting from the first fastener. An equal load distribution between the fasteners for multiple fastener joints was assumed. For solving the system of equations resulting from the boundary conditions of the model the program mathematica was used. As the boundary conditions lead to quite difficult expressions due to the used shape function (7), the program was only able to solve the system of equations for given values of the studied variables. Contrary to a FE-calculation these solutions are analytical and not numerical.

The influence of the geometry on the energy release rate G_I for a crack extension from $x_1 = -d$ until $x_1 = -1{,}5 \cdot d$ ($\Delta a = d / 2$) was then studied by fitting a non-linear regression to the numerous results (equation (10)):

$$G_I = 1{,}275 \cdot 10^{-6} \cdot n^{0.155} \cdot d^{0{,}639} \cdot \rho^{2{,}00} \cdot \left(\frac{a_1}{d}\right)^{-0{,}710} \cdot \left(\frac{a_3}{d}\right)^{-0{,}302} \cdot \left(\frac{a_4}{d}\right)^{-0{,}074} \quad [N/mm] \quad (10).$$

For equation (10) only models with more than one fastener in a row were used ($n \geq 2$).

In the studied models mode 1b according to Johansen was assumed. Equation (10) may conservatively also applied for timber members, where the fastener remains straight and is inclined. For timber members, where a plastic hinge occurs in the fastener, equation (10) can easily be extended:

$$G_I = 1{,}275 \cdot 10^{-6} \cdot n^{0.155} \cdot d^{0{,}639} \cdot \rho^{2{,}00} \cdot \left(\frac{a_1}{d}\right)^{-0{,}710} \cdot \left(\frac{a_3}{d}\right)^{-0{,}302} \cdot \left(\frac{a_4}{d}\right)^{-0{,}074} \cdot \frac{y^2}{t^2} \quad [N/mm] \quad (11),$$

where

$$y = F_{Johansen} / (f_h \cdot d) = F_{Johansen} / (0{,}082 \cdot (1 - 0{,}01 \cdot d) \cdot \rho \cdot d) \quad (12),$$

$F_{Johansen}$ = load-carrying capacity per dowel per shear plane according to Johansen

t timber thickness,
n number of fasteners in a row,
d fastener diameter,
ρ density,
a_1 distance between fasteners in a row,
a_3 fastener end distance,
a_4 fastener edge distance.

The criterion for crack extension resulting from (11), (12) is

$$G_c \leq G_I = \frac{F_{Johansen}^2 \cdot 1{,}275 \cdot 10^{-6} \cdot n^{0.155} \cdot d^{0{,}639} \cdot \left(\frac{a_1}{d}\right)^{-0{,}710} \cdot \left(\frac{a_3}{d}\right)^{-0{,}302} \cdot \left(\frac{a_4}{d}\right)^{-0{,}074}}{(0{,}082 \cdot (1 - 0{,}01 \cdot d) \cdot d)^2 \cdot t^2} \quad [N/mm] \quad (13)$$

with the critical energy release rate G_c as a property of resistance.

If equation (13) is not fulfilled the resistance per fastener per shear plane has to be limited according to equation (14):

$$F_{Jo\_red\_1} = \sqrt{\frac{G_c \cdot (0{,}082 \cdot (1 - 0{,}01 \cdot d) \cdot d)^2 \cdot t^2}{1{,}275 \cdot 10^{-6} \cdot n^{0.155} \cdot d^{0{,}639} \cdot \left(\frac{a_1}{d}\right)^{-0{,}710} \cdot \left(\frac{a_3}{d}\right)^{-0{,}302} \cdot \left(\frac{a_4}{d}\right)^{-0{,}074}}} \; [N] \qquad (14)$$

with $n \geq 2$.

A similar equation was fitted taking also into account models with one fastener ($n \geq 1$), the distance a_1 between the fasteners is then obviously not included:

$$F_{Jo\_red\_2} = \sqrt{\frac{G_c \cdot (0{,}082 \cdot (1 - 0{,}01 \cdot d) \cdot d)^2 \cdot t^2}{0{,}331 \cdot 10^{-6} \cdot n^{0.248} \cdot d^{0{,}634} \cdot \left(\frac{a_3}{d}\right)^{-0{,}290} \cdot \left(\frac{a_4}{d}\right)^{-0{,}210}}} / [N] \qquad (15)$$

with $n \geq 1$.

Equations (14) and (15) are compared to the empirically found result of Jorissen (1998) which was transformed resulting in the load per fastener per shear plane assuming equal load distribution within the fasteners in a row :

$$F_{Jorissen\_1} = 0{,}37 \cdot n^{-0{,}1} \cdot \left(\frac{a_1}{d}\right)^{0{,}30} \cdot (\lambda)^{0{,}20} \cdot F_{Johansen} \qquad (16)$$

with

$$\lambda = \min \begin{cases} t_m / d & t_m: \text{ thickness of the middle member} \\ 2 \cdot t_s / d & t_s: \text{ thickness of the side member} \end{cases} \qquad (17)$$

and $F_{Johansen}$ the load carrying capacity per fastener and shear plane according to Johansen.

As the equation according to Jorissen is based on tests including joints with one fastener, the effect of numbers of fastener n in a row is taken into account using equation (15) and (16). The resulting exponent of n according to equation (15) is:

$$n^{-0{,}248 \cdot 1/2} = n^{-0{,}124} \qquad (18)$$

which is in good agreement to Jorissen's exponent of -0,1.

Using the variables of equation (19) and assuming equal load distribution within the fasteners the diagram in fig. 9 shows the effect of the number of fasteners n per row. The shape of the curves according to (14), (15) and (16) is quite similar. The difference in the values might be caused by the assumption of equal load distribution within the row, an effect which is included in Jorissen's empirically based equation. Furthermore the variation of the embedding strength is included in (16) but not in (14) and (15) using equation (12).

$$\rho = 450\ \mathrm{kg/m^3} \qquad f_y = 240\ \mathrm{N/mm^2}$$
$$M_y = \frac{f_y \cdot d^3}{6} \qquad t_1 = \frac{d}{\sqrt{6}} \cdot \sqrt{\frac{f_y}{f_h}}$$
$$t_2 = 3 \cdot t_1 \qquad d = 24$$
$$a_1 = 7 \cdot d \qquad a_3 = 7 \cdot d \qquad (19)$$
$$a_4 = 3 \cdot d \qquad G_c = 0{,}214\ \mathrm{Nmm/mm^2}$$
$$\beta = \frac{f_{h,2}}{f_{h,1}} = 1 \qquad \lambda = \frac{2 \cdot t_1}{d}$$

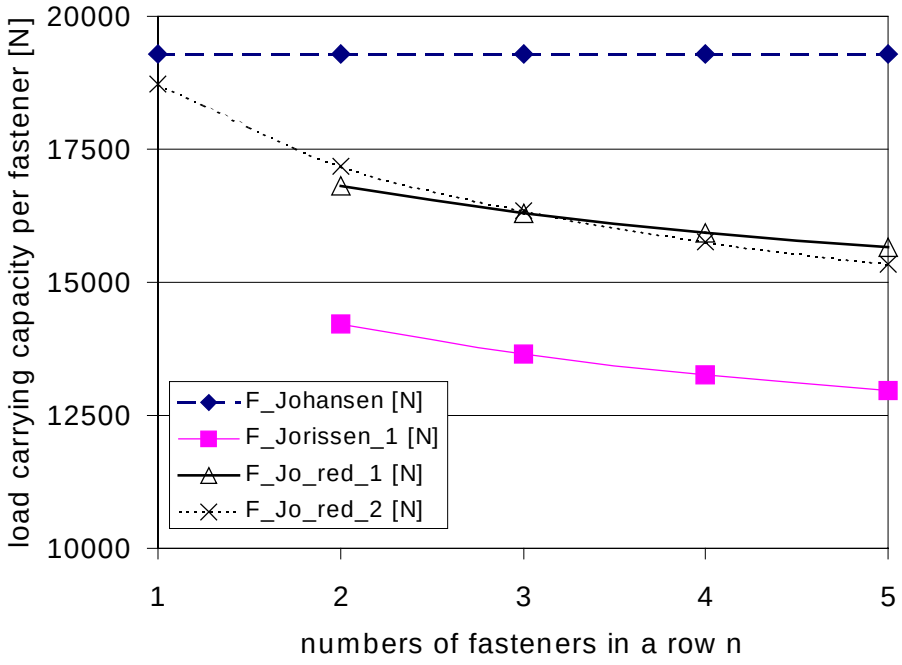

Fig. 9: effect of the number of fasteners per row

Fig. 10 and fig. 11 show the influence of the diameter on the load carrying capacity which is not included in Jorissen's investigations as only 20 from 958 tests had a diameter different from 12 mm.

Values used for fig. 10

$$\rho = 450\ \mathrm{kg/m^3} \qquad f_y = 240\ \mathrm{N/mm^2} \qquad M_y = \frac{f_y \cdot d^3}{6} \qquad t_1 = \frac{d}{\sqrt{6}} \cdot \sqrt{\frac{f_y}{f_h}}$$
$$t_2 = 3 \cdot t_1 \qquad n = 3 \qquad a_1 = 7 \cdot d \qquad a_3 = 7 \cdot d \qquad (20)$$
$$a_4 = 3 \cdot d \qquad G_c = 0{,}214\ \mathrm{Nmm/mm^2} \qquad \beta = \frac{f_{h,2}}{f_{h,1}} = 1 \qquad \lambda = \frac{2 \cdot t_1}{d}$$

Values used for fig. 11:

$$\rho = 450\ \mathrm{kg/m^3} \qquad f_y = 240\ \mathrm{N/mm^2} \qquad M_y = \frac{f_y \cdot d^3}{6} \qquad n = 3$$

$$t_1 = \frac{2+\sqrt{2}}{\sqrt{6}} \cdot d \cdot \sqrt{\frac{f_y}{f_h}} \qquad t_2 = t_1 \qquad a_1 = 7 \cdot d \qquad a_3 = 7 \cdot d \qquad (21)$$

$$a_4 = 3 \cdot d \qquad G_c = 0{,}214\ \mathrm{Nmm/mm^2} \qquad \beta = 1 \qquad \lambda = \frac{2 \cdot t_1}{d}$$

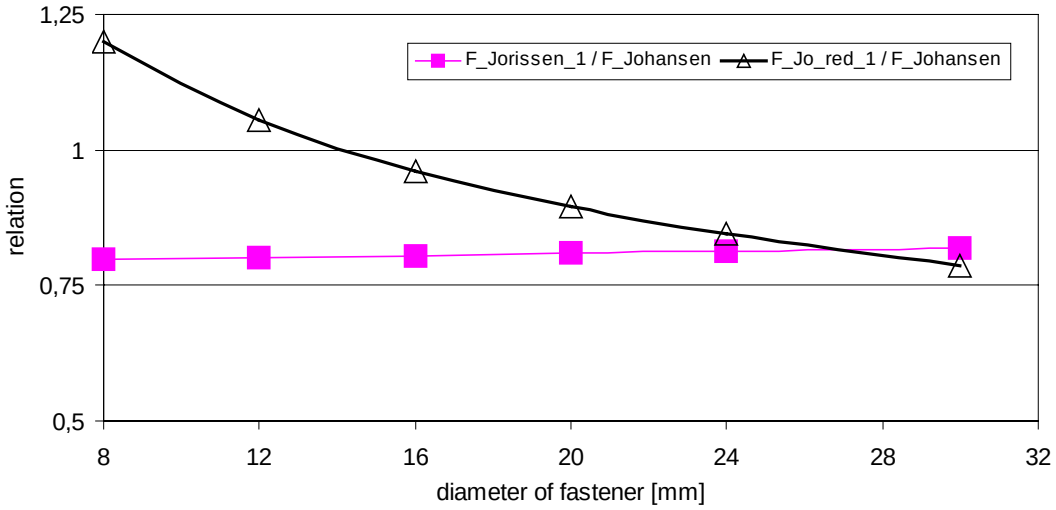

Fig. 10: effect of diameter with a constant slenderness leading to failure mode 1b, properties according to (20)

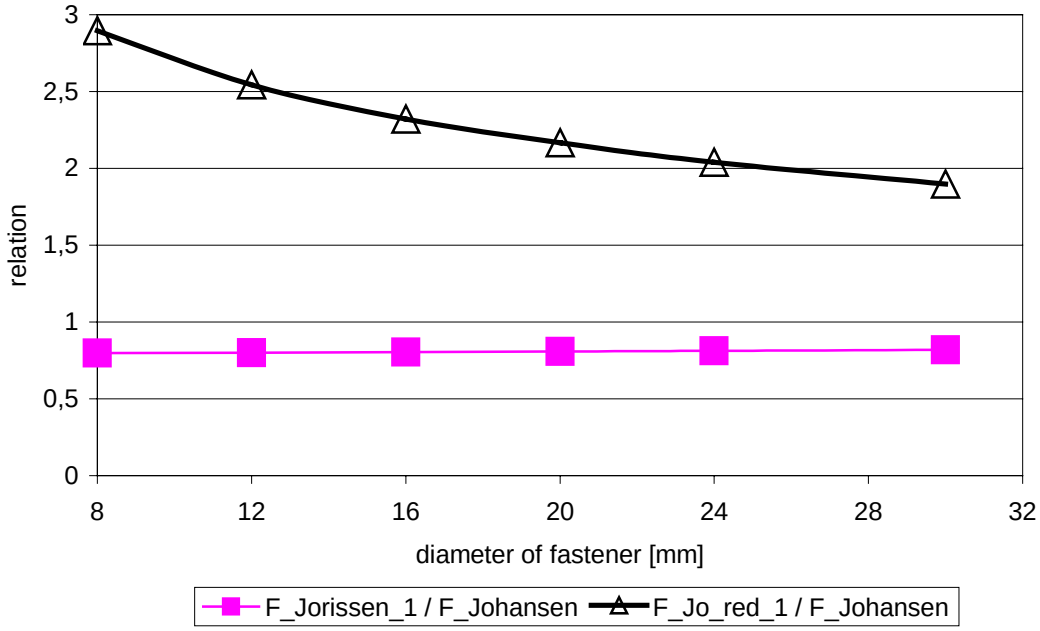

Fig. 11: effect of diameter with a constant slenderness leading to failure mode 3, properties according to (21)

According to fig. 11 splitting would hardly occur if Johansen's failure mode 3 is governing.

Fig. 12 to 14 show the effect of the joint geometry according to equations (14) and (15). The properties were those of (20) except for the variables. The diameter was d = 16 mm.

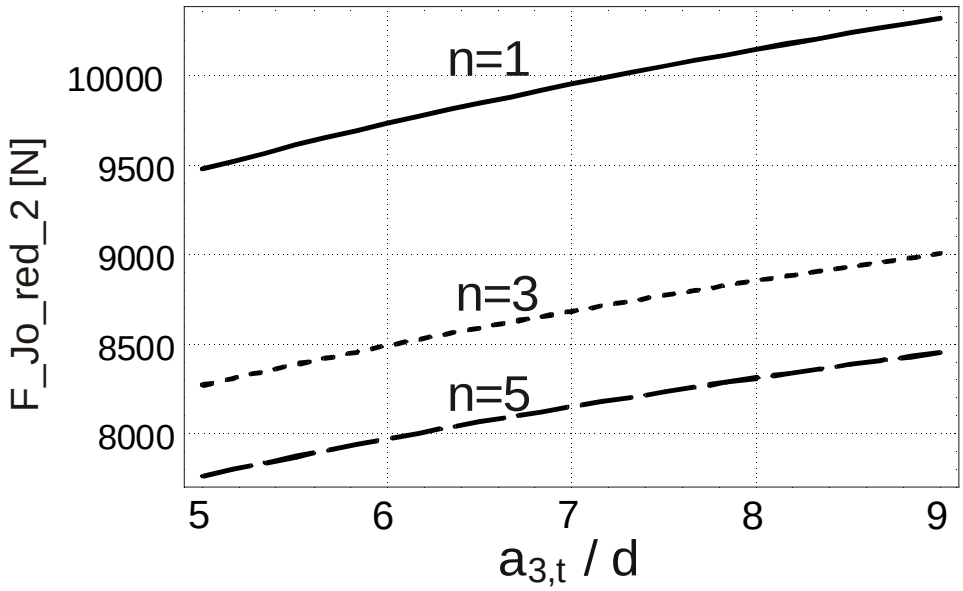

Fig. 12: effect of end distance $a_{3,t}$

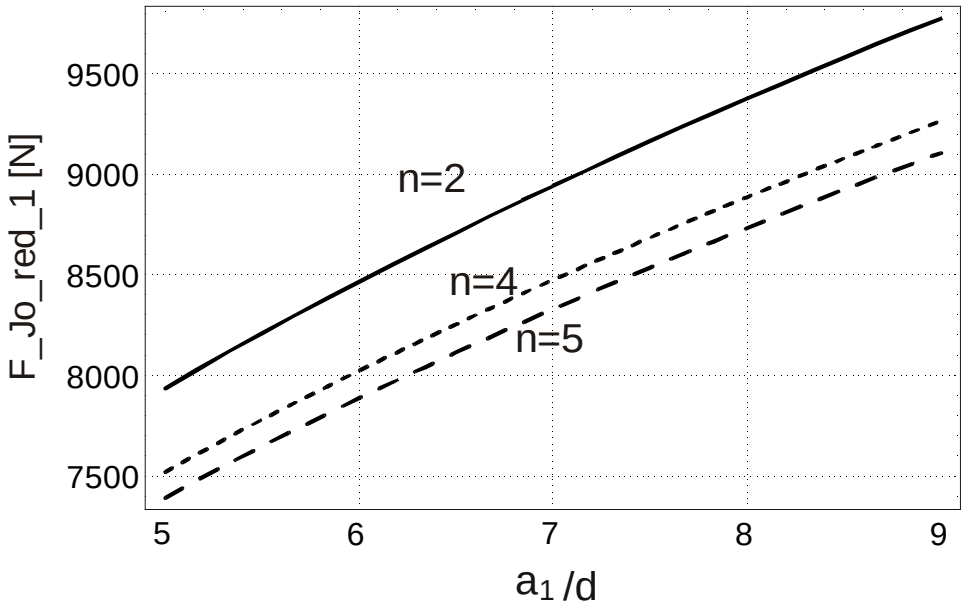

Fig. 13: effect of spacing a_1

The most favourable influence has therefore an increase of the fastener spacing a_1.

Increasing the edge distance increases the load carrying capacity of a single fastener joint (fig. 14). Figures 12 to 14 are based on the fitted equations based on numerous calculations of the energy release rate. If figures 12 to 14 would directly be based on the calculation of energy release rates for the configurations considered, the influence of the parameters would be even more pronounced.

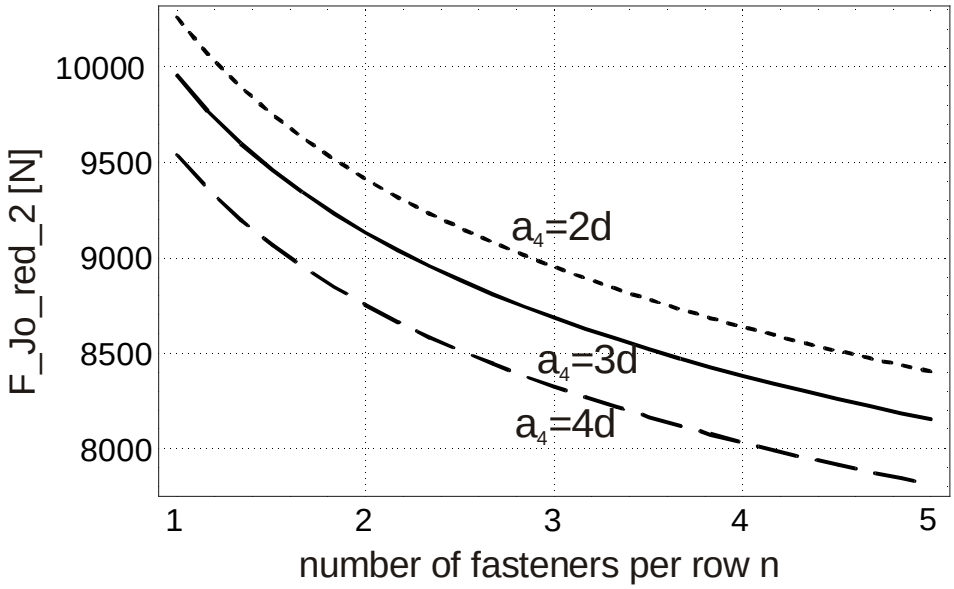

Fig. 14: effect of edge distance $a_{4,c}$

4. Conclusions

The influence of geometry and material properties on the splitting tendency in the connection area of timber members was studied using a fracture mechanics approach. Based on the results of this approach, the model developed by Jorissen (1998) was modified. The predictions of the load-carrying capacity of multiple fastener joints show a good agreement with the test results of Jorissen. The effect of joint geometry was also studied using the model. The major influencing parameter on the splitting tendency of timber in the connection area is the fastener spacing a_1 parallel to the grain, while $a_{3,t}$ and $a_{4,c}$ are of minor influence for joints with more than one fastener. For similar geometry and the same fastener slenderness the absolute diameter has a significant influence as well. Joints, where failure mode 3 according to Johansen's yield theory governs the design should hardly fail by timber splitting.

Further research is necessary for the group tear failure or plug shear failure. These failure modes are a combination of mode I and II crack extension. If mode I dominates, however, the results should be similar those presented here.

Literature

Blaß, H.J.; Schmid, M. (2002). Spaltgefahr von Nadelhölzern. Versuchsanstalt für Stahl, Holz und Steine, Abteilung Ingenieurholzbau, Universität Karlsruhe (TH). In German.

Masuda, M. (1998). Fracture analysis of bolted joints using the finite small area criterion. Fifth World Conference on Timber Engineering. Montreux. Volume I, S. 321-328

Jorissen, A.J.M. (1998). Double Shear Timber Connections with Dowel Type Fasteners. Delft University Press, Delft, 1998.

Timoshenko, S.P. und Goodier, J.N. (1970). Theory of Elasticity. 3. Edition, McGraw-Hill Book Company, Singapore.

Quenneville, P. (1998)Predicting the failure modes and strength of brittle bolted connections. 5th World conference on timber engineering, Montreux, Switzerland.

Mohammad, M.; Quenneville, P. (1999). Behaviour of wood-steel-wood bolted glulam connections. CIB-W18, paper 32-7-1, Graz, Austria.